

CHARACTERISTICS OF FLOW THROUGH THROTTLING VALVE UNDERGOING A STEEP PRESSURE GRADIENT

Xin Fu¹, Xuewen Du¹, Jun Zou¹, Hong Ji², Shohei Ryu³ and Masami Ochiai³

¹State Key Laboratory of Fluid Power Transmission and Control, Zhejiang University, Hangzhou 310027, China

²School of Fluid Power & Control Engineering, Lanzhou University of Technology, Lanzhou 730050, China

³Technical Research Laboratory, Hitachi Construction Machinery Co. Ltd. Tsuchiura. Ibaraki. Japan

Abstract

This paper presents predictions and measurements of the structures of cavitation flow inside the throttling valve. The three-dimensional Navier-Stokes equations in a moving reference frame are solved on tetrahedral meshes. A sliding mesh technique is utilized to characterize unsteady interactions. The accuracy of the predicted flow fields is evaluated by comparison to measurement results taken with a high-speed camera. Results show that the pressure distribution inside the throttling groove is sensitive to the valve port configuration and flow direction. Bubbles form near the side wall of the groove on the throttling edge where, in the case of flow into the throttling groove, the pressure is at a minimum. With the increase of the pressure gradient bubbles saturate the flow. Noise spectrum analysis indicates that the noise level induced by cavitation is determined by the number and size of the bubbles passing through the valve grooves.

Keywords: pressure distribution, CFD, valve, cavitation, noise

1 Introduction

Cavitation can be generated by the passage of fluid through a constriction such as a throttling valve etc. If the throttling is sufficient to cause the pressure around the point of vena contracta to fall below the threshold pressure, millions of bubbles are generated. Subsequently, as the liquid jet expands and the pressure recovers the bubbles collapse.

Cavitation causes problems in fluid power systems and components. When actions for preventing cavitation are considered, it is essential to recognize the exact mechanism driving cavitation. As is well known, the pressure distribution inside the flow area is the primary factor which determines the formation and development of cavitation, so it is fundamentally important to study the cavitation phenomenon in fluid power systems and the relationship between the pressure distributions and the cavitation noise caused by the breakup of bubbles.

Several investigations concerning the cavitation phenomenon have previously been accomplished (He, 1995; Totten, 1998; Arcoumanis, 1998, 1999; Nagasaka, 2000, Warjito, 2002). Additionally, many studies on cavitation in hydraulic valves have been done. Martin et al., (1981) investigated cavitation inception a

spool valve and analyzed the relation between flow pattern, jet orientation and energy spectra. Oshima et al., (2001) investigated the effects of cavitation on the characteristics of flow rate, noise level, pressure distributions and the inception of cavitation in water hydraulic poppet valves.

Various indirect methods such as CFD analysis and numerical simulations are applied (Shih, 1995; Spalart, 2000). Reynolds (1976) and Launder (1990) provided some numerical methods on the study of turbulent flow. Pountney et al., (1989) numerically studied the flow patterns and pressure variations within the valve orifice based on the $k-\varepsilon$ turbulence model. It is clear that the pressure difference, flow direction and geometrical shape of the valve (orifice) play an important role in the formation of bubbles and the cause of noise. The relationship of these factors, however, is not yet clear, due to the complexities of the physical processes of the internal flow in the valve and the environment into which the jet is injected.

In this paper both a numerical simulation and an experimental investigation were undertaken to study the high-speed flow field in oil hydraulic systems. The objective of the study is to determine the effects of pressure difference, flow direction and valve port con-

This manuscript was received on 26 July 2006 and was accepted after revision for publication on 12 February 2007

figuration on noise due to bubble generation in the flow through the valve. As a result, cavitation phenomenon is explained and the effects of cavitation on the system are discussed.

2 Experimental Equipments and Theoretical Model Setup

2.1 Pressure Measurement

When liquid passes through the metering groove of a spool valve the kinetic energy/velocity of the liquid increases as the pressure decreases. If the throttling is sufficient to cause the pressure around the point of vena contracta to fall below the threshold pressure for cavitation, or saturated vapor pressure, millions of bubbles are generated. Subsequently, as the liquid jet expands and the pressure recovers the bubbles collapse. During the passage of the liquid through the constriction, boundary layer separation occurs and a substantial amount of energy is lost in the form of a pressure drop. It is vitally important, therefore, to test the pressure variation in the narrow metering groove areas in order to discover the mechanism driving cavitation inception and development.

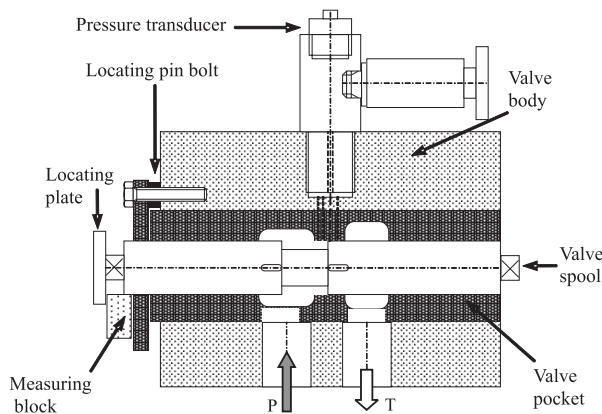


Fig. 1: Pressure distribution measurement apparatus

Pressure distributions near the metering grooves are tested by the apparatus shown in Fig. 1. Metering grooves are symmetrically distributed on the two sides of the spool lands. The valve spool and locating plate are connected with screws. The measuring blocks are located between the locating plate and the valve pocket. Changing the thickness of the measuring blocks determines the valve openings. Pressure transducers are fixed on the taps that open on the surface of the valve body. Three rows of pressure taps with 0.6 mm or 1 mm diameters (shown in Fig. 2) are located in the valve pocket. The valve pocket can move in the axial direction and revolve around the axis in the valve body so that each of the pressure taps can connect with the pressure transmitter. A more detailed explanation of the facility and the method of measuring pressure distribution inside the valve is illustrated by Ji et al. (2004). Locating the position of the valve pocket is determined by locating the pin bolts. Back pressure is adjusted through the back pressure valve.

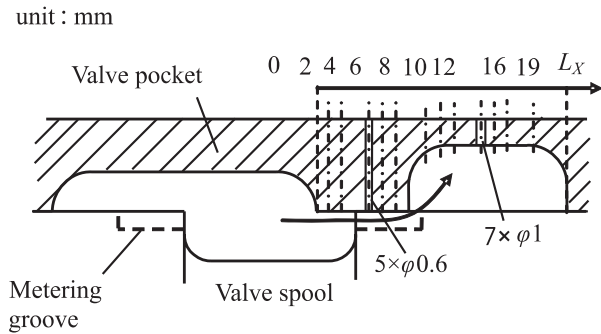


Fig. 2: Pressure taps in axial direction

Some strategies are taken to prevent the unfavorable effects of cavitation on the flow field inside the valve chamber.

- The diameter of the pressure taps near the throttling groove ($\phi 0.6$ mm) is smaller than those in the valve chamber ($\phi 1$ mm).
- The figure of the inlet/outlet oil-holes is elliptical and oil-holes in the valve body are larger than those in the valve pocket. This guarantees that the oil-return resistance will not change when the valve pocket moves or revolves.
- The pressure taps are arranged in long rows. This guarantees a reliable seal and, when one tap connects with the pressure transducer, it will not be disturbed by other taps.

The transducer used to measure the pressures at the inlet is Germany BOSCH (0-35 MPa) and the absolute pressure transducer used to measure the pressure distribution near the metering groove is a PHS-50KA (Japan KYOWA) (0-5 MPa abs.).

2.2 Cavitation Observation and Noise Measurement

The noise level measurement and image acquisition system is schematically shown in Fig. 3. The sound pressure level of noise was measured with a AWA6270 noise analyzer and cavitation observation was made by a high-speed video camera (FASTCAM-ultima APX by PHOTRON Limited) with a maximal speed of 120,000 frames per second. The size of the imaging area depends on the recording speed. For example, a speed of 24,000 fps allows for an image size of 512×256 pixels. Images are stored as a sequence of 8 bit (256 levels) digital monochrome pictures that can be recorded to a normal video cassette recorder or to the computer storage.

The video controller has a trigger input to hold the current sequence of the recorded images. By triggering the video controller when an impulsive force had been measured by an appropriate sensor, sequential pictures of bubbles under various pressure differences were taken which corresponded to the fluctuation of inlet pressure and noise tested by the noise analyzer.

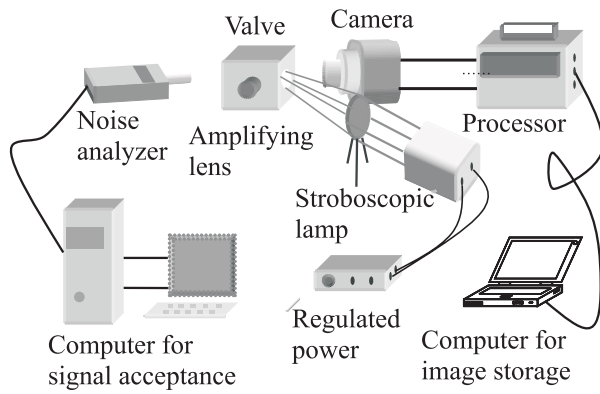


Fig. 3: High speed observation and noise testing system

For easy observation the valve body is made of transparent Plexiglass (polymethyl methacrylate-PMMA). The configuration of the flow passage is the same as the pressure measurement apparatus shown in Fig. 1 except that the diameters of the inlet and outlet oil-holes are smaller (12 mm). Compared to the throttling area A_0 as shown in Fig. 4, the flow area of the oil-holes $A_H \gg A_0$. The slight variation, therefore, of the inlet (outlet) oil-holes will not affect the flow field inside the valve. The cavitation bubbles are observed through the Plexiglass using a non-stroboscopic light to illuminate the inside of the valve.

2.3 Theoretical Model

Different types of valve spools were systematically studied in this paper. All spool grooves have the same length ($L = 5 \text{ mm}$) and end radius ($r = 1 \text{ mm}$). The only difference is the groove depth (H) (Fig. 4). The tests are carried out in two different flow directions, “flow-in” and “flow-out”. In the case of flow-in (IN), as shown by the spool position in Fig. 5, the oil stream flows through the groove to the oil-return chamber at the small valve opening (x). In the case of flow-out (OUT), the spool moves from the left up until the right two notches at the throttling position.

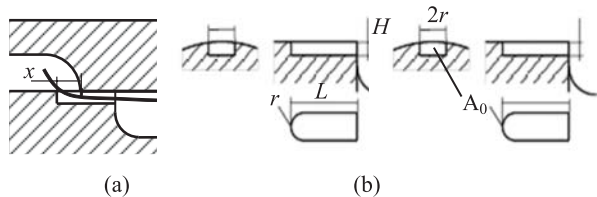


Fig. 4: Throttling groove configuration

The internal structure of a three-dimensional geometry model used in computation is shown in Fig. 5. The simulation is carried out under a constant inlet pressure of 3 MPa and outlet pressure of 0.98 MPa. Under this critical pressure the flow inside the valve tunnel is assumed to be turbulent and the fluid is considered incompressible with constant properties. The velocity and pressure in the turbulent flow can be decomposed into an average and pulsating quality respectively:

$$u_i = U_i + u_i' \quad (1)$$

$$p_i = P_i + p_i' \quad (2)$$

For incompressible flow, the Reynolds continuity equation is expressed by

$$\frac{\partial U_i}{\partial x_i} = 0 \quad (3)$$

Neglecting the mass force, and substituting Eq. 1 and Eq. 2 into the Navier-Stokes momentum equation results in

$$\frac{\partial U_i}{\partial t} + U_j \frac{\partial U_i}{\partial x_j} = -\frac{1}{\rho} \frac{\partial P}{\partial x_i} + \nu \frac{\partial^2 U_i}{\partial x_i \partial x_j} + \frac{1}{\rho} \frac{\partial (-\overline{\rho u_i' u_j'})}{\partial x_j} \quad (4)$$

The kinetic control equation (or Reynolds equation) is similar to the laminar N-S equation for the average pressure and molecular viscous force, except for an additional stress called the Reynolds stress $-\overline{\rho u_i' u_j'}$. The Reynolds equation is not enclosed because the parameter is unknown, so the $k-\varepsilon$ turbulent model should be introduced in order to obtain the solution to the equation. The Renormalization Group $k-\varepsilon$ (RNG $k-\varepsilon$) model is adopted to solve the problem. The numerical model is described in (FLUENT, 2003). The SIMPLE algorithm is employed in calculating the pressure and velocity fields because it showed good convergent characteristics as the grids became finer. During the calculation, the residuals are used to monitor the convergence of the solution.

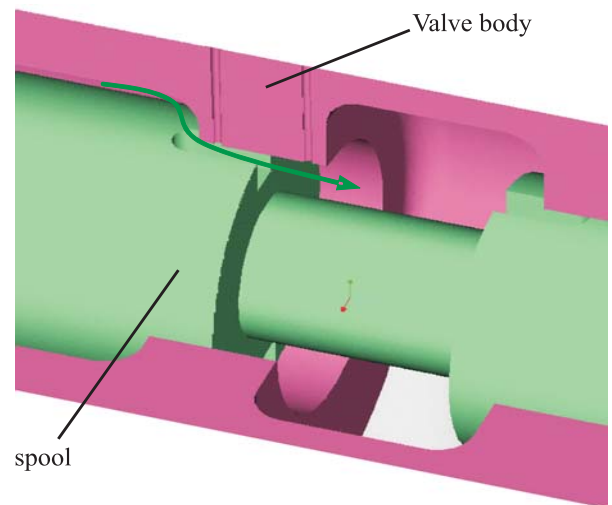


Fig. 5: Structural model and flow tunnel inside valve

Due to the symmetrical structure inside the valve body, only half of the flow field requires model building and mesh division. The governing equations were discretized in both space and time on tetrahedral meshes based on the unstructured finite-volume method. Smaller meshes were adopted near the metering grooves because of the higher gradient of pressure and velocity near these grooves. Other areas adopt a larger mesh so as to increase the computational efficiency. The local mesh division near the metering groove is demonstrated in Fig. 6. The stability and the convergence of the simulation are greatly influenced by the number of grid cells and their distributions. The optimum grid structure in the current study was selected and a sufficiently fine grid size having 140,000~200,000 grid points was adopted in the com-

putational domain based on different groove types. At least 5 grid cells are guaranteed on the shortest edge of the grooves.

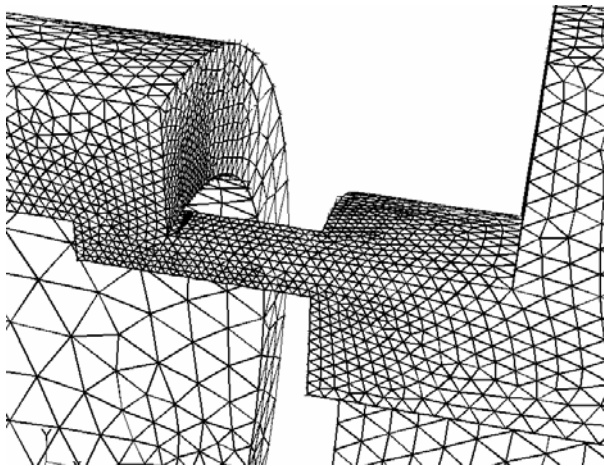


Fig. 6: Mesh division of the throttling groove

Boundary conditions were set according to the experiment: the inlet boundary was set as the type of pressure inlet and the outlet boundary was set as the pressure outlet. The span of values was corresponded with experimental conditions. During the simulation and calculation oil density ρ was 889 kg/m^3 , and dynamic viscosity ν was $4 \times 10^{-5} \text{ m}^2/\text{s}$.

3 Simulations Results

3.1 Flow-Out

As shown in Fig. 7, there is a clear pressure drop at the inlet area of the metering groove ($x = 2 \text{ mm}$). There are two main characteristics in the flow passage. One is the uniform-section between the inlet and outlet of the groove and the other is the turning area near the sharp inlet (outlet) corner. Both resist the flow and result in a pressure loss. This characteristic of the flow passage, however, can also lift the pressure near the sharp inlet corner of the groove and avoid cavitation.

The stream contracts near the inlet area A_{10} and the pressure drops rapidly. Pressure at the turning point B (1.2 MPa) is the minimum pressure near the inlet area. Cavitation, therefore, occurs more easily here and the increasing of pressure near point B can effectively avoid cavitation. The other stream turning area is the outlet of the groove where local pressure drops from 1.97 MPa (point C) to 0.9 MPa (point F) because of elbow effects.

Oil flows to the return chamber through area A_2 , where reflux vortices take place. At the same time, flow velocity decreases along the flow direction. The lowest pressure (point E, F: 0.9 MPa) appears behind the sharp corner area where the stream separation takes place. The low-pressure area is another place where cavitation inception appears.

With the increase of groove depth as shown in Fig. 8, pressure losses inside the throttling passage decrease. The pressure distribution is more sensitive to

the flow contraction and stream turning at the inlet area. Pressure drops near the area A_2 increase (1.63 MPa-1.01 MPa), but the positions of low pressure area remain unchanged. This corresponds with the vortex shedding area at the turning points. As the valve opening increases the pressure losses inside the groove gradually disappear.

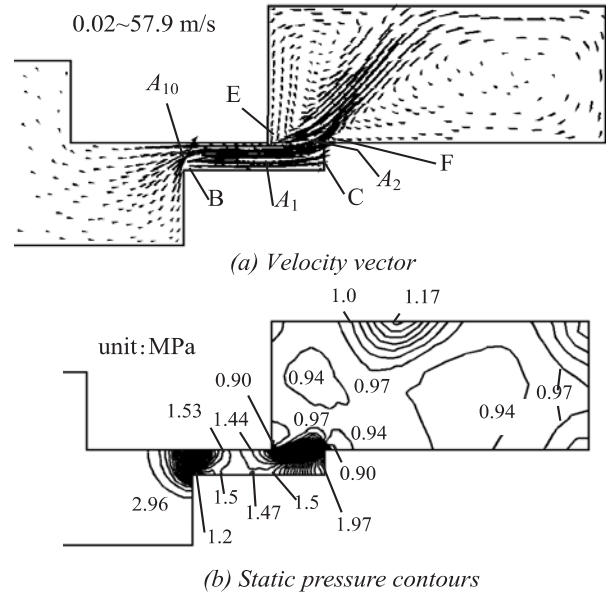


Fig. 7: Velocity vector and pressure contours inside groove, $x = 2.0 \text{ mm}$, $H = 1.0 \text{ mm}$, OUT

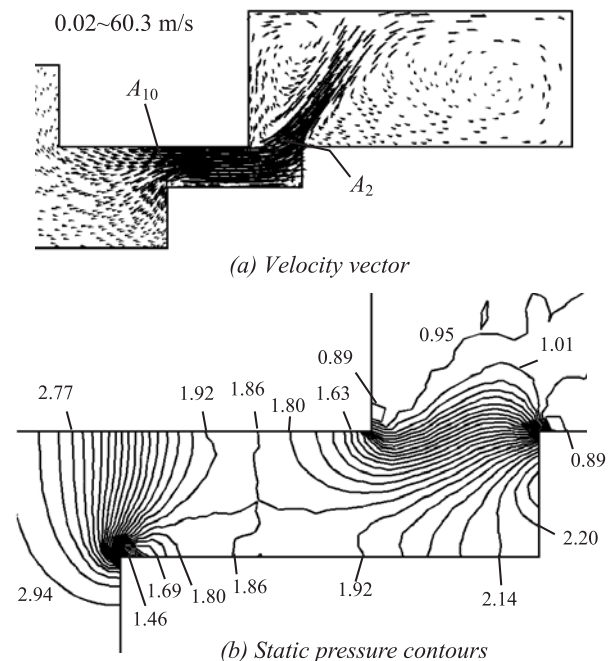


Fig. 8: Velocity vector and pressure contours inside groove, $x = 2.0 \text{ mm}$, $H = 1.5 \text{ mm}$, OUT

3.2 Flow-In

The velocity vector and pressure contours in the case of flow-in are demonstrated in Fig. 9. These figures clearly show that the pressure drop occurs mainly at the inlet corner of the groove. The minimum pressure appears at point D where the flow separation takes place.

When the valve opening is 2 mm, the radial distribution of pressure inside the groove is also shown in Fig. 9 (b). The lowest pressure (0.44 MPa) is located at the side wall of the groove which is even lower than the pressure in point D. The inception of cavitation is also prone to occurring here.

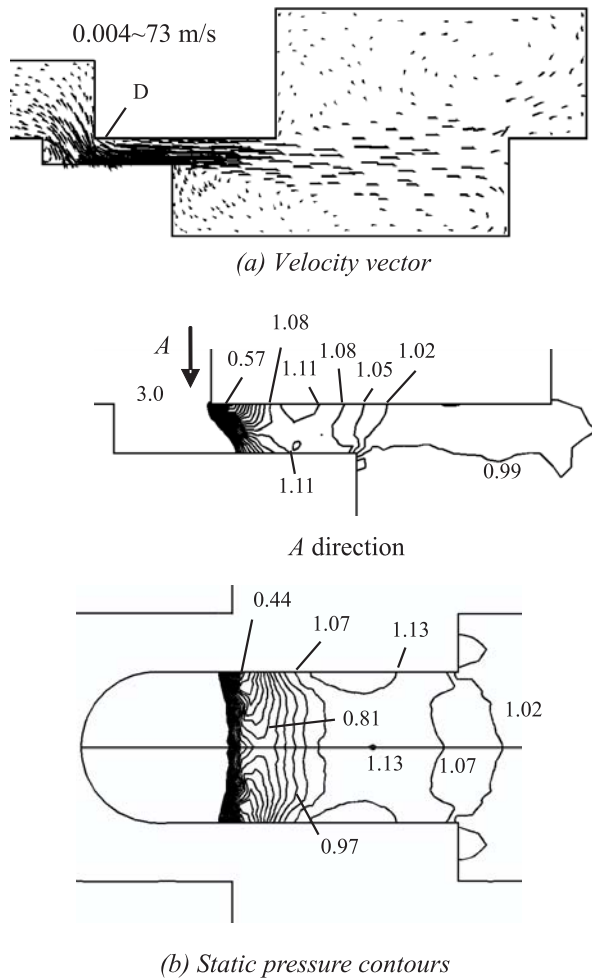


Fig. 9: Velocity vector and pressure contours inside groove, $x=2.0$ mm, $H=1.0$ mm, IN

There are two main differences between flow-in and flow-out. The first is the pressure drop gradient on the inlet area of the groove. The pressure drop is greater in the case of flow-in (3-0.57 MPa) than in the case of flow-out (2.96-1.2 MPa). This will induce more intense cavitation. The second difference is the pressure distribution near the outlet area. There is no sharp pressure drop in the case of flow-in.

As the valve opening increases, the length of the uniform-section between the inlet and outlet area becomes shorter and the resistance along the flow direction decreases. As a result pressure recovery becomes slower.

4 Experimental Verification

4.1 Pressure Distribution

The apparatus used for pressure measurement inside the throttling valve is shown in Fig. 10. To guarantee the

comparable conditions between simulation and measurement, the inside configuration of the experiment valve is the same as the simulation model shown in Fig. 5. The measuring structure and method are shown in Fig. 1 and Fig. 2. Detailed descriptions of the facility and the method of measuring the pressure distribution inside the valve are illustrated in (Ji, 2004). During all measurements the input temperature of the oil was kept constant at 40° C.



Fig. 10: Photo of experimental apparatus

Figure 11 shows a comparison of the simulation and experimental results for different valve openings (groove depth $H = 1.5$ mm) in the case of flow-out. The experimental results agree with the simulation. There is an obvious two-stage pressure drop when the valve opening is small ($x = 1$ mm). The drop areas are consistent with the position where the pressure contours are dense (shown in Fig. 8).

By increasing the valve opening x , the inlet flow area shifts to the right and the outlet area increases correspondingly. Pressure-drops near the outlet area decrease rapidly and pressure-drops near the inlet area sharply increase. Further increasing the valve opening area results in the valve opening no longer being able to throttle. The metering groove is prone to be a thin wall orifice. At $L_x = 7$ mm, the inlet high pressure drops to back pressure (see the location of the coordinate system shown in Fig. 2). Pressure variations at other groove depths yield similar results.

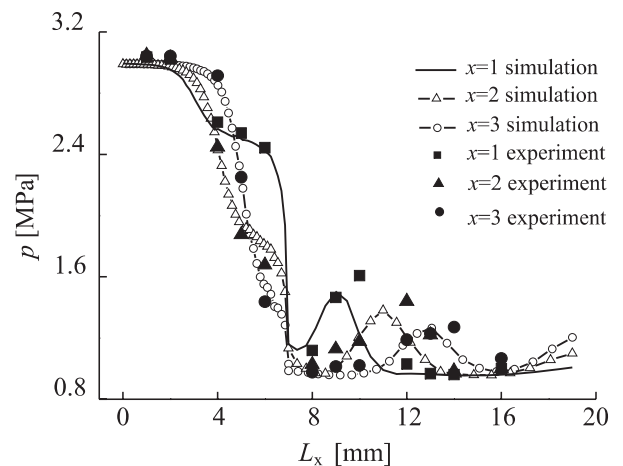


Fig. 11: Pressure distributions inside throttling groove, $p_1 = 3$ MPa, $p_2 = 0.98$ MPa, OUT

Pressure fluctuations arise inside the flow passage with increasing groove depth in the case of flow-out because of the relatively higher jet flow velocities. While in the case of flow-in, the regularities of pressure distributions are very similar in different depths and different valve openings of metering grooves (see Fig. 12). The main characteristic is the pressure overshoot at the inlet corner of the valve port which can effectively retard the formation and growth of bubbles due to shedding inside the groove. With the increase of groove depth, pressure overshoots decrease rapidly.

The minimum value of pressure occurs at $L_x = 7$ mm in the case of flow-out and $L_x = 0.2$ mm in the case of flow-in as shown in Fig. 11 and Fig. 12. These two locations are both the sharp inlet corners of the valve port in either flow direction. The inception and development of cavitation are considered to generate near these areas.

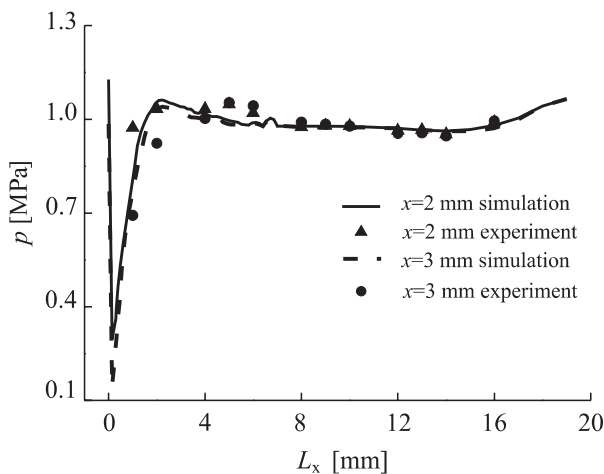


Fig. 12: Pressure distributions inside throttling groove, $p_1 = 3$ MPa, $p_2 = 0.98$ MPa, IN

4.2 Cavitation Noise

It is difficult to observe the cavitation flow inside the valve because the flow velocity near the groove is very high under the steep pressure gradient. For easier observation of cavitation, some researchers have enlarged the transparent model or simplified the valve structure. But the flow field varies over a wide range due to the change of structural shapes. At the same time, scaling effects will introduce additional unfavorable conditions due to cavitation. For these reasons prototype valve observation is still adopted here.

Images of cavitation were obtained by the high-speed camera in macro-shot mode. At the same time, the sound pressure level (*SPL*) of noise was measured. The noise analyzer was placed 50 mm away from the valve body.

Although the formation of bubbly flow inside the groove is different under different flow directions, valve openings, and pressure gradients, the main characteristic is similar. Millions of bubbles form at the inlet area of the throttling edge. Very high intensity fluid turbulence then becomes present downstream of the constriction; its intensity depends on the magnitude of the pressure drop, which, in turn, depends on the

geometry of the constriction and the flow conditions of the liquid. Subsequently, as the liquid jet expands and the pressure recovers, the bubbles collapse.

In the case of flow-out, the cavitation appearances are similar at different valve openings under the same pressure gradient and groove depth. Figure 14 shows cavitation in full-development under the pressure difference of 3 MPa ($H = 2$ mm, $x = 4$ mm). It is found that a long, cloud-like vortex appears downstream and collapses near the groove exit. The shedding pattern has a periodic character though it does not always last in perfect regularity for a long time and can change with variations in the groove depth or valve openings. Due to the two-level pressure drop inside the groove (Fig. 11), no serious noise induced by cavitation is detected.

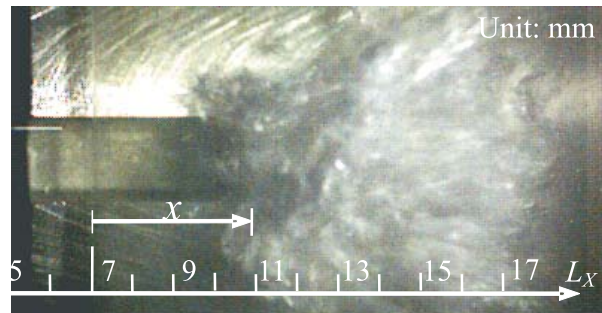


Fig. 13: Characteristic of cavitation appearance, OUT

The primary feature of cavitation flow in the case of flow-in is shown in Fig. 14. Flow velocity varies from 60 to 100 m/s depending on the inlet pressure p_1 . Due to the high velocity gradient and the vena contracta of flow, boundary layer separation occurs and a substantial amount of energy is lost in the form of a pressure drop. (Fig. 12). Cavitation inception occurs mainly at the sharp-edged area along the side-wall of the groove because of the shear strength between the high-velocity flow and the solid boundary. The shear strength will lead to even lower pressure near the inlet area (Fig. 9) and induce large-scale cavitation vortices. With the rush of flow bubbly-lines are formed.



Fig. 14: Characteristic of cavitation appearance, IN

The effect of pressure distribution on cavitation inception inside the groove is shown in Fig. 15 ($H = 2$ mm, $x = 2$ mm). Pressure distribution inside the groove is mainly affected by the back pressure p_2 . When p_2 falls below a certain pressure (1 bar), the orifice is filled with an intense flow of saturation bubbles as shown in Fig. 15(a). There are also large quantities of micro-bubbles floating outside the groove in the chamber which can be seen with the high camera-shot speed (24,000 fps). The sound pressure level (*SPL*) of noise under this situation is relatively high (83.6 dB).

With the increase of back pressure, floating bubbles disappear and the length of bubbly flow decreases rapidly. The rail of jet flux (collapse area) moves to the outlet area inside the valve chamber (Fig. 15(b)). At the same time the maximum value of noise appears (85.3 dB, $p_2 = 4$ bar). When p_2 reaches 0.8 MPa, small bubbles appear and disappear intermittently along the surface of the side-wall in the downstream throttling edge. The bubbles travel downstream for short distances and disappear rapidly near the outlet of the orifice (Fig. 15(c)). This can be defined as the criterion for cavitation inception and will be discussed later. Noise level start to be lower in this situation (82.4 dB, $p_2 = 8$ bar). When p_2 is increased further, bubbles disappear completely and the noise level is reduced below 80 dB rapidly.

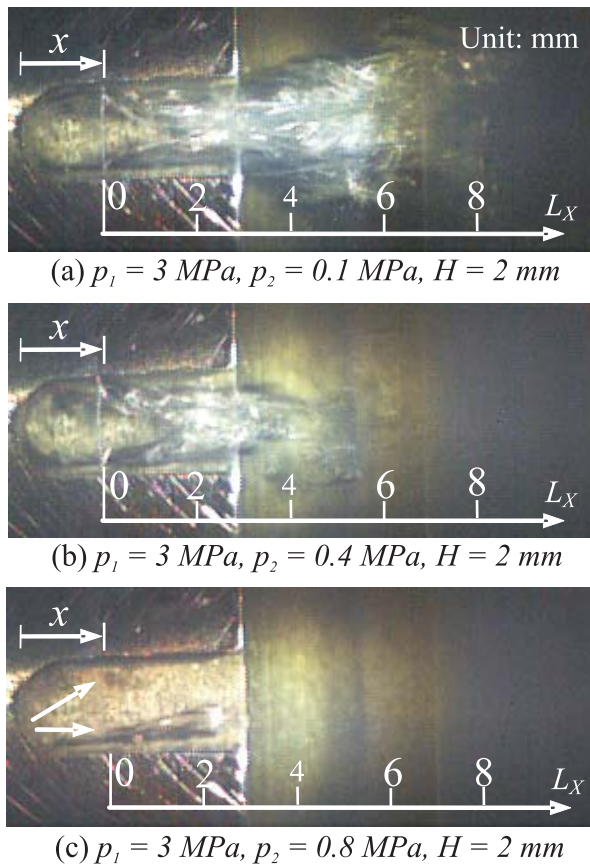


Fig. 15: Cavitation appearance under different back pressure p_2 ($p_1 = 3$ MPa, $x = 2$ mm), IN

The variation of sound pressure levels under different valve openings ($H = 2$ mm, $p_1 = 3$ MPa) are compared in Fig. 16. When $p_2 < 0.3$ MPa, noise levels decrease with the increase of valve openings. With the increase of back pressure, the noise level in larger valve openings ($x = 4$) increases rapidly. As the back pressure increases further, the noise level decreases sharply with the reduction of cavitation inside the groove. The larger the valve opening, the faster the noise level disappears. This phenomenon indicates that the pressure distribution near the groove is the key factor which determines the cavitation noise level in the valve because the flow in the larger valve opening is more sensitive to the variations of back pressure.

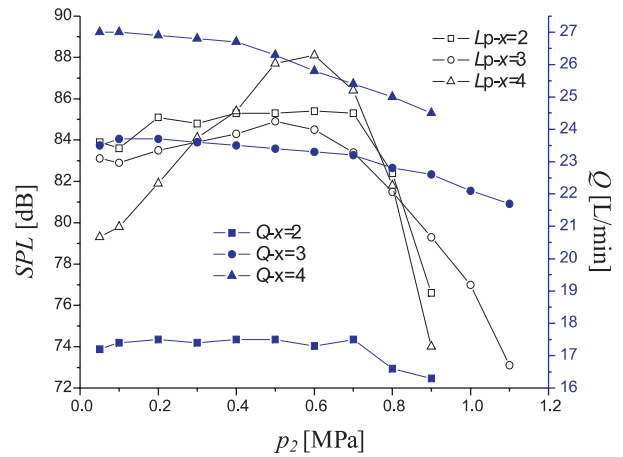


Fig. 16: Noise and flow under different valve openings ($p_1 = 3$ MPa)

The variations of flow rate under different valve openings are recorded and shown in Fig. 16. As the valve openings increase, flow rates increase correspondingly. The regularity of variation is not in accordance with the variation of noise level. This result indicates that flow rate is not the major factor which determines the cavitation noise level inside the valve.

The variation in the appearance of bubbles for different values of inlet pressure is also investigated. It is found that the cavitation pattern is not very sensitive to the minor difference in the inlet pressure. The inlet pressure mainly affects the saturation degree of bubbly flow inside the groove and affects the intensity of the sound pressure level accordingly.

5 Discussion

The highest noise levels will not appear when the bubbly flow is the most intense (Fig. 15, 16). The reason for this that the interaction between each bubble reduces the pressure intensity when millions of bubbles collapse. One conclusion can be drawn from the phenomenon, that the quantity of bubbles is not necessarily the key factor which determines the noise level due to cavitation flow. Preliminary study of the spectrum analysis demonstrates that the dominant frequency of noise will increase when back pressure increases (Fig. 17). This implies that the bubble size may be another main factor which determines the level of cavitation noise. Investigation of the relationship between bubble shapes and noise spectrum is a main task in future studies in order to discover the mechanism driving cavitation noise.

The inception of cavitation is extremely difficult to define because of small openings, high velocities and relatively small bubbles. Attempts have been made to formulate a criterion for the definition of incipient cavitation by (Martin 1981), by comparing the ratio of cavitating spectra to noncavitating spectra. The high level of jet noise, however, makes it difficult to distinguish between noise caused by cavitation and noise caused by other sources and the bubbles at cavitation inception are difficult to observe.

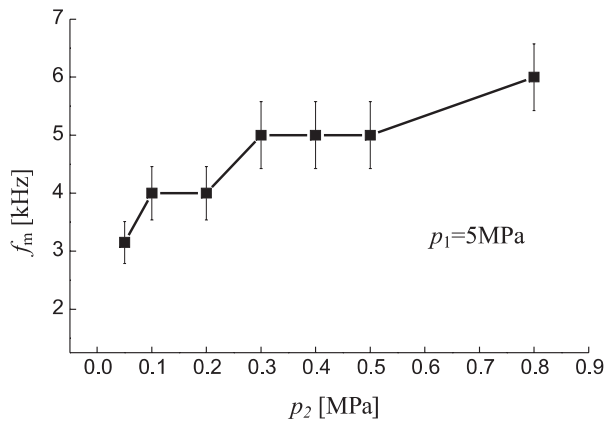


Fig. 17: Dominant frequency shift with back pressure ($H = 1.5$ mm, $x = 2$ mm)

To develop the research, we adopt a transparent model and a high speed camera to observe the onset of cavitation. The characteristic appearance is shown in Fig. 15(c). Back pressure $p_2 = 0.8$ MPa is the critical pressure for cavitation inception under the inlet pressure $p_1 = 3$ MPa ($H = 2$ mm). As the back pressure increases further, bubbles vanish completely and noise level drops to ambient noise level. Comparing with Fig. 9(b) and Fig. 12, the area of cavitation inception corresponds to the area of minimum pressure. The simulation model is reliable to predict cavitation in valve grooves. But as to two phase flow, and the effect of cavitation on the flow field, the SST $k-\omega$ model is better. The comparison of two models in the application of cavitation flow is underway, and the results will be provided in the near future.

6 Conclusion

A computational analysis using RNG $k-\epsilon$ model and an experimental analysis using a high-speed camera were conducted to obtain a better understanding of the characteristics of cavitation flow inside the throttling valve. The major conclusions obtained in the present study can be summarized as follows:

In comparison with high-speed observation results, reliable results in the predictions of the cavitation flow patterns inside the grooves were obtained.

Cavitation inception is prone to take place near the turning corner of the throttling edge where pressure is at a minimum. The bubbles saturate the flow and a choking phenomenon in the cavitation flow exists when pressure near the groove falls below a certain pressure. With the increase of back pressure, cavitation disappears gradually, but the noise level reaches a peak before it disappears.

The dominant frequency of noise will increase when back pressure increases. This implies that the quantity of bubbles is not necessarily the key factor which determines the sound pressure level of cavitation noise. Other factors such as bubble size, collapsing intensity and shear wave of high-velocity bubbly flow are of equal importance. Due to the complexities of the physical processes of the internal flow in the valve, details of the cavitation mechanism are still under investigation through numerical modeling as well as further experiments.

Nomenclature

A_H	Flow area of oil-holes	[mm ²]
A_0	Throttling area	[mm ²]
A_{10}	Inlet area of groove	[mm ²]
A_2	Outlet area of groove	[mm ²]
H	Groove depth	[mm]
L	Groove length	[mm]
r	End radius of grooves	[mm]
x	valve opening	[mm]
u'_i	fluctuation velocity in the i direction	[m/s]
u'_j	fluctuation velocity in the j direction	[m/s]
μ_t	viscosity coefficient of vortices	
U_i	average velocity in the i direction	[m/s]
U_j	average velocity in the j direction	[m/s]
ν	Dynamic viscosity of oil	[m ² /s]
ρ	Fluid density	[kg/m ³]
Q	Flow discharge inside the groove	[L/min]
L_p	Noise level of cavitation flow	[dB]
p_1, p_2	inlet and outlet pressure	[MPa]

Acknowledgements

The authors are grateful to the National Grand Fundamental Research Program of China (973 Program) (No. 2006CB705405) and National Natural Science Foundation of China (Project Number: 50575200) for the financial support.

References

- Arcoumanis, C. and Gavaises, M. 1998. Linking nozzle flow with spray characteristics in a diesel fuel injection system. *Atom Sprays*, Vol. 8, pp. 307-47.
- Arcoumanis, C., Flora, H., Gavaises, M., Kampanis, N. and Horrocks, R. 1999. Investigation of cavitation in a vertical multi-hole diesel injector. *SAE Paper* 1999-01-0524.
- Martin, C. S., Medlarz, H., Wiggert, D. C. and Brennen, C. 1981. Cavitation inception in spool valve. *Journal of fluid engineering, Transaction of the ASME*, Vol.103, pp. 564-574.
- FLUENT, *User's Guide Version 6*, Fluent Inc., 2003.
- He, L. and Ruiz, F. 1995. Effect of cavitation on flow and turbulence in plain orifices for high-speed atomization. *Atom Sprays*, Vol. 5, pp. 69-84.
- Ji, H., Fu, X., Yang, H. Y. and Wang, Q. F. 2004. Measurement on pressure distribution of non-circular opening spool valve. *Chinese journal of mechanical engineering*, Vol. 40, pp. 99-102.
- Nagasaka, K., Takagi, T., Koyanagi, K. and Yamachi, T. 2000. The development of fine atomization injector. *JSAE Review*. Vol. 21, pp. 309-313.
- Oshima, Sh., Leino, T., Linjama, M., Koskinen, K. T. and Vilenius, M. J. 2001. Effect of cavitation in

water hydraulic poppet valves. *International Journal of Fluid Power*, Vol. 2, pp. 5-13.

Shih, T., Liu, W., Shabir, A., Yang, Z. and Zhu, J. 1995. A New $k-\epsilon$ Eddy Viscosity Model for High Reynolds Number Turbulence Flows. *Comput. Fluids*, Vol. 24, pp. 227-238.

Spalart, P. 2000. Strategies for Turbulence Modelling and Simulations. *Int. J. Heat Fluid Flow*, Vol. 21, pp. 252-263.

Totten, G. E., Suny, H., Bishop, J. and Xie L. 1998. Hydraulic system cavitation: a review. *SAE transactions*, Vol. 107, pp. 368-380.

Warjito, O. and Mochizuki, M. Kiya. 2002. Bubbly Flow Undergoing a Steep Pressure Gradient. *Exp Fluids*, Vol. 33, pp. 620-628.

Pountney, D. C., Weston, W. and Banieghbal, M. R. 1989. A numerical study of turbulent flow characteristics of servo-valve orifices. *Proceedings of the Institution of Mechanical Engineers. Part A. Power and process engineering*. Vol. 203, pp. 139-147.

Renolds, W. C. 1976. Computation of turbulent flows. *Annual Rev. Fluid Mech.*, Vol. 8, pp. 183-208.

Lauder, B. E. and Spalding, D. B. 1990. The numerical computation of turbulent flows. *Computer Methods in Applied Mechanics and Engineering*. pp. 269-289.



Xin Fu

Born in 1961, he is a Prof. Dr. in the Mechatronic Department within the Mechanical Engineering college at Zhejiang University, P. R. China. He is also the Director of the State Key Lab of Fluid Power Transmission and Control at Zhejiang University. His main research areas are computation fluid dynamics in hydraulic components, fluid power transmission, MEMS and vibration/noise control in hydraulic valves. He has published more than 100 papers in technical journals and at international conferences.



Xuewen Du

Born in June, 1978, he received his M. Sc from Gaungxi University (China) in 2004. He is currently a graduate student pursuing a doctoral degree at the State Key Lab of Fluid Power Transmission and Control at Zhejiang University. His primary research fields are fluid visualization in hydraulic components and fluid noise control.



Zou Jun

Born in July, 1977, he received his PhD from the Zhejiang University (China) in 2006. He is currently a researcher at the State Key Lab of Fluid Power Transmission and Control at Zhejiang University. His primary research is electrohydraulic servo systems.



Hong Ji

Born in 1972, he received his PhD from Zhejiang University in 2005 and is currently an associate Prof. at Lanzhou University of Technology, P.R. China. His main research fields are fluid noise and vibration control, motor-pump and mobile hydraulics. He has published more than 20 papers. At present, his research is supported by Nature Science Foundation of China and Nature Science Foundation of Gansu Province.